Optical phonon production by upconversion: Heterojunction-transmitted versus native phonons

Seungha Shin and Massoud Kaviany

Optical phonon production by upconversion: heterojunction-transmitted versus native phonons

Seungha Shin[*]

Department of Mechanical, Aerospace and Biomedical Engineering,

University of Tennessee, Knoxville, Tennessee 37996, USA

Massoud Kaviany

Department of Mechanical Engineering,

University of Michigan, Ann Arbor, Michigan 48109, USA

(Dated: April 13, 2015)

Abstract

High-energy optical phonons are preferred in phonon-absorbing transitions, and regarding their production we analyze the phonon upconversion processes under nonequilibrium created by heterojunction transmission. For heterojunction, steady phonon flux from low cut-off frequency layer (e.g., Ge) is transmitted to high cut-off layer (e.g., Si), creating nonequilibrium population of low-energy phonons for upconversion. Using quantum spectral phonon transmission and first-principles calculations of the phonon interaction kinetics, we identify the high conversion efficiency channels, i.e., modes and wavevectors. Junction-transmitted phonons, despite suffering from the interface reflection and from spreading interactions with the equilibrium native phonons, have high upconversion rate to Brillouin zone-boundary optical phonons, while the nonequilibrium native phonons are efficiently upconverted over most of the zone. So, depending on the harvested optical phonon, one of these nonequilibrium phonons can be selected for efficient upconversion rate.

PACS numbers: 63.20.kg, 74.25.Kc, 79.60.Jv

[*] sshin@utk.edu

I. INTRODUCTION

Phonons emitted by transiting and transitioning of energy carriers in solid, create local nonequilibrium population which will consequently equilibrate by phonon-electron (p-e) [1], phonon-spin (p-s) [2], and phonon-phonon (p-p) interactions [3]. The p-p processes dominate with increased temperature and include phonon up- and downconversion, where in three-phonon upconversion two phonons are annihilated creating one phonon with higher energy (E_p) (reverse in downconversion) [4]. The upconversion can be explored for resonant optical phonon source, analogous to photon upconversion, in which sequential absorption of two or more photons leads to emission of one with higher energy [5]. The photon upconversion is used in infrared-to-visible conversion (e.g., in lasers) and in optical storage, although the efficiency is rather low [6], where the quantized electromagnetic wave interacts with electric (or magnetic) entities leading to metastable excited states [7].

The p-p interaction kinetics is determined by the anharmonicity in the force field and the phonon population distribution under the conservation of momentum and energy. The up- and downconversion rates are balanced under equilibrium. So, for a desirable interaction characteristic (e.g., enhanced phonon upconversion under its absorption in energy conversion), the population distribution needs a controlled deviation from the equilibrium. We examine heterojunction structure for providing distinct nonequilibrium phonon population near the interface. We note that in homogeneous bulk solids this deviation from equilibrium is only noticeable under extreme local heating (different from heterojunction transmission).

In this article, based on the interaction kinetics of the low-energy phonon upconversion, we introduce a heterojunction phonon upconverter (HPUC) for efficient supply of optical phonons which have higher energy and lower entropy. The high-energy, optical phonons can be harvested in unassisted resonant electronic transitions (phonon-tuned heterobarrier [8]) and in phonon-assisted photon absorption processes in semiconductors and in isolated rare-earth ions [9, 10]. Other applications of resonance (optical) phonon absorption can include infrared (IR) photon emission as the reverse of the IR two-phonon emission [11, 12], i.e., using phonon upconversion in enhanced IR optical source. In these applications, the harvested optical phonons are absorbed and converted to electronic energy.

In the HPUC system, the low-energy phonons cross the junction into a high-energy layer (creating overpopulation), upconvert there and then become absorbed (with steady under-

population of high-energy phonons). This upconversion of the transmitted phonons is also compared with nonequilibrium phonons in a bulk solid (native phonons) through heat flux. We use the Ge/Si junction as example, establish the method and calculations of phonon interaction kinetics from the first principles, describe the need for nonequilibrium populations and the role of heterojunction in providing them, and define the process efficiency. Nonequilibrium phonon population and their interaction kinetics have been extensively studied in phonon transport [13, 14]. Since the objective has been relaxation time related to phonon scattering (resistance), rather than energy conversion among the phonon modes, the detailed nonequilibrium population distribution need not be addressed. To our best knowledge, this study is the first on the relaxation processes with separate consideration of the up- and downconversions and estimation and manipulation of nonequilibrium phonon population distribution.

II. UPCONVERSION KINETICS

The potential energy in the crystal Hamiltonian [H $= \langle \varphi \rangle + \sum_i (\boldsymbol{p}_i^2 / 2M_i)$, where $\sum_i (\boldsymbol{p}_i^2 / 2M_i)$ is the total kinetic energy (i: atomic index, M_i: mass, $\boldsymbol{p}_i$: momentum)] is considered for the phonon properties and interaction kinetics and expressed as [3, 4]

$$\langle \varphi \rangle = \langle \varphi \rangle_\mathrm{o} + \frac{1}{2!} \sum_{ijxy} \Gamma_{ij}^{xy} d_i^x d_j^y + \frac{1}{3!} \sum_{ijkxyz} \Psi_{ijk}^{xyz} d_i^x d_j^y d_k^z + \dots, \tag{1}$$

where $\langle \varphi \rangle_\mathrm{o}$ is the equilibrium potential energy, d_i^x is the displacement of atom i (or j, k) in x (or y, z) coordinate (Cartesian), and Γ and Ψ are the second- and third-order (cubic) force constants.

Phonons are identified with the wavevector $\boldsymbol{\kappa}$ [in the first Brillouin zone (BZ)] and mode α, and their energy ($E_{p,\boldsymbol{\kappa}\alpha}$) and crystal momentum ($\boldsymbol{p}_{p,\boldsymbol{\kappa}}$) are respectively $\hbar\omega_{\boldsymbol{\kappa}\alpha}$ and $\hbar\boldsymbol{\kappa}$, where $\hbar$ is the reduced Planck constant and $\omega_{\boldsymbol{\kappa}\alpha}$ is the angular frequency of phonon $\boldsymbol{\kappa}\alpha$. For the phonon energy or frequency with respect to $\boldsymbol{\kappa}$ and α, we employ the equation of motion for a plane wave using the dynamical matrix $\boldsymbol{D}$,

$$\omega_{\boldsymbol{\kappa}}^2 \boldsymbol{e}_{\boldsymbol{\kappa}} = \boldsymbol{D}(\boldsymbol{\kappa}) \boldsymbol{e}_{\boldsymbol{\kappa}}. \tag{2}$$

Here, an element $D_{ij}^{xy}(\boldsymbol{\kappa})$ of $\boldsymbol{D}(\boldsymbol{\kappa})$ is calculated using the second derivatives,

$$D_{ij}^{xy}(\boldsymbol{\kappa}) = \frac{1}{(M_i M_j)^{1/2}} \sum_m \Gamma_{il,jm}^{xy} \exp[i\boldsymbol{\kappa} \cdot (\boldsymbol{r}_{jm} - \boldsymbol{r}_{il})], \tag{3}$$

3

where M_i is the atomic mass of i-th atom, $\Gamma_{il,jm}^{xy}$ is the second-order force constant of the interaction between i-th atom in l-th unit cell and j-th atom in m-th unit cell, and $\boldsymbol{r}_{jm}$ is the position vector of j-th atom in m-th unit cell. The phonon angular frequency is obtained from the eigenvalue in Eq. (2), and the number of modes depends on the matrix dimension. Both Ge and Si considered here have six phonon modes due to two atoms in the primitive cell, i.e., longitudinal acoustic (LA), two transverse acoustic (TA1 and TA2, $E_{p,\mathrm{TA1}} < E_{p,\mathrm{TA2}}$), longitudinal optical (LO), and two transverse optical (TO1 and TO2, $E_{p,\mathrm{TO1}} < E_{p,\mathrm{TO2}}$).

The kinetics of the p-p interactions are studied with the anharmonic (greater than the second order) terms in Eq. (1), and among the interactions, the three-phonon up- and downconversions depend on the cubic force constants. Higher-order interactions have also been considered [15–18], but the interaction rate decreases as the order increases. The four-phonon interaction rates are negligible compared to three-phonon interactions [17], so the phonon relaxation time is primarily that of the three-phonon interactions (although the quartic terms can affect the shift in the phonon frequency) [18]. The four possible interactions involving phonon $\boldsymbol{\kappa}\alpha$ are shown in Fig. 1, and through interaction with $\boldsymbol{\kappa}'\alpha'$ and $\boldsymbol{\kappa}''\alpha''$, phonon $\boldsymbol{\kappa}\alpha$ is created (A and B) or annihilated (C and D), conserving energy and crystal quasi-momentum (with transitional invariance [19]).
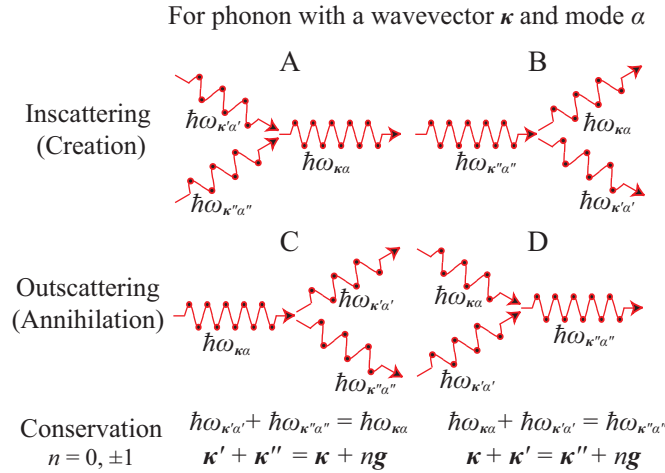
FIG. 1. Three-phonon processes involving phonon of wavevector $\boldsymbol{\kappa}$ and mode α interacting with $\boldsymbol{\kappa}'\alpha'$ and $\boldsymbol{\kappa}''\alpha''$, where $\boldsymbol{\kappa}\alpha$ is created (A and B) or annihilated (C and D), with energy and momentum ($\boldsymbol{g}$ is reciprocal lattice vector) conservations.

The three-phonon interaction rate of the phonon $\boldsymbol{\kappa}\alpha$ (per primitive cell per second), from the Fermi golden rule [20], is

$$\dot{\gamma}_{\boldsymbol{\kappa}\alpha} = \sum_{\alpha'\alpha''} \frac{\hbar\pi}{16} \iint_{\mathrm{BZ}} |\Psi_{\alpha\alpha'\alpha''}^{\boldsymbol{\kappa\kappa'\kappa''}}|^2 \Delta_{\boldsymbol{\kappa\kappa'\kappa''}} \delta(\omega_{\boldsymbol{\kappa}\alpha}, \omega_{\boldsymbol{\kappa'}\alpha'}, \omega_{\boldsymbol{\kappa''}\alpha''}) f_{pop}(f_{p,\boldsymbol{\kappa}\alpha}, f_{p,\boldsymbol{\kappa'}\alpha'}, f_{p,\boldsymbol{\kappa''}\alpha''}) \mathrm{d}\boldsymbol{\kappa'}\mathrm{d}\boldsymbol{\kappa''}. \quad (4)$$

Here, the three-phonon interaction element $\Psi_{\alpha\alpha'\alpha''}^{\boldsymbol{\kappa\kappa'\kappa''}}$ is given by [20]

$$\Psi_{\alpha\alpha'\alpha''}^{\boldsymbol{\kappa\kappa'\kappa''}} = \sum_{ijk} \sum_{xyz} \frac{\varepsilon_{xi}^{\boldsymbol{\kappa}\alpha} \varepsilon_{yj}^{\boldsymbol{\kappa'}\alpha'} \varepsilon_{zk}^{\boldsymbol{\kappa''}\alpha''}}{(M_i M_j M_k \omega_{\boldsymbol{\kappa}\alpha} \omega_{\boldsymbol{\kappa'}\alpha'} \omega_{\boldsymbol{\kappa''}\alpha''})^{1/2}} \Psi_{ijk}^{xyz} \exp\left[i(\boldsymbol{\kappa}\cdot\boldsymbol{r}_i + \boldsymbol{\kappa'}\cdot\boldsymbol{r}_j + \boldsymbol{\kappa''}\cdot\boldsymbol{r}_k)\right], \quad (5)$$

where $\varepsilon_{xi}^{\boldsymbol{\kappa}\alpha}$ is the component x of the eigenvector $\boldsymbol{e_\kappa}$ [from Eq. (2)] for mode α and atom i, and Ψ_{ijk}^{xyz} is the third-order derivatives in Eq. (1). $\Delta_{\boldsymbol{\kappa\kappa'\kappa''}}$ ensures momentum conservation and is unity when $(\boldsymbol{\kappa}-\boldsymbol{\kappa'}-\boldsymbol{\kappa''})$ for interactions A and C or $(\boldsymbol{\kappa}+\boldsymbol{\kappa'}-\boldsymbol{\kappa''})$ for B and D in Fig. 1 is 0 or $\pm\boldsymbol{g}$ (reciprocal lattice vector); otherwise zero. $\delta(\omega_{\boldsymbol{\kappa}\alpha}, \omega_{\boldsymbol{\kappa'}\alpha'}, \omega_{\boldsymbol{\kappa''}\alpha''})$ is a delta function of angular frequency change ($|\omega_{\boldsymbol{\kappa}\alpha}-\omega_{\boldsymbol{\kappa'}\alpha'}-\omega_{\boldsymbol{\kappa''}\alpha''}|$ for A and C, $|\omega_{\boldsymbol{\kappa}\alpha}+\omega_{\boldsymbol{\kappa'}\alpha'}-\omega_{\boldsymbol{\kappa''}\alpha''}|$ for B and D), and is treated with the adaptive broadening scheme [21]. $f_{p,\boldsymbol{\kappa}\alpha}$ is the occupancy of the phonon $\boldsymbol{\kappa}\alpha$, and $f_{pop}(f_{p,\boldsymbol{\kappa}\alpha}, f_{p,\boldsymbol{\kappa'}\alpha'}, f_{p,\boldsymbol{\kappa''}\alpha''})$ is the product of $f_{p,\boldsymbol{\kappa}\alpha(\mathrm{or}\ \boldsymbol{\kappa'}\alpha',\boldsymbol{\kappa''}\alpha'')}$ (annihilation) or $f_{p,\boldsymbol{\kappa}\alpha(\mathrm{or}\ \boldsymbol{\kappa'}\alpha',\boldsymbol{\kappa''}\alpha'')} + 1$ (creation) [e.g. for process A, $f_{pop} = (f_{p,\boldsymbol{\kappa}\alpha} + 1)f_{p,\boldsymbol{\kappa'}\alpha'} f_{p,\boldsymbol{\kappa''}\alpha''}$], so the up- and downconversion rates are the same under equilibrium occupancies {Bose-Einstein $f_{p,\boldsymbol{\kappa}\alpha}^{\mathrm{o}}(\omega_{\boldsymbol{\kappa}\alpha}, T) = [\exp(\hbar\omega_{\boldsymbol{\kappa}\alpha}/k_{\mathrm{B}}T) - 1]^{-1}$, k_{B}: Boltzmann constant, T: temperature}. In numerical integration of kinetics, we use $27 \times 27 \times 27$ Monkhorst-Pack -point grid (560 points representing 19683 points in first BZ) [22].

The dynamical (or second-order) and the third-order force constant matrices are calculated using the density functional perturbation theory (DFPT) [23] with the first-order perturbation (by $2n + 1$ formula [24]). The structure relaxation and the unperturbed electron wavefunction calculations using the density functional theory (DFT) precede the phonon calculations. The Quantum Espresso package with the norm-conserving pseudopotential in Perdew-Zunger local density approximation is employed for these DFT and DFPT calculations [25].

The creation (cr)/annihilation (an) rate of specific phonon hp (harvested phonon) is calculated by integrating the change rate of hp population during $\boldsymbol{\kappa}\alpha$-phonon interactions [Eq. (4)] over all wavevectors $(\boldsymbol{\kappa})$ and modes (α). The net rate of change of phonon hp

population $\dot{n}_{hp}$ and energy $\dot{s}_{hp}$ per unit volume are

$$\dot{n}_{hp} = \dot{n}_{hp,cr} - \dot{n}_{hp,an} = \frac{1}{8\pi^3} \sum_s \sum_\alpha \int_{\text{BZ}} \dot{\gamma}_{\boldsymbol{\kappa}\alpha,s} \Delta_{\boldsymbol{\kappa}\alpha,hp,s} \mathrm{d}\boldsymbol{\kappa} \qquad \text{and}$$

$$\dot{s}_{hp} = \dot{s}_{hp,cr} - \dot{s}_{hp,an} = \frac{1}{8\pi^3} \sum_s \sum_\alpha \int_{\text{BZ}} \dot{\gamma}_{\boldsymbol{\kappa}\alpha,s} \Delta_{\boldsymbol{\kappa}\alpha,hp,s} \hbar\omega_{hp} \mathrm{d}\boldsymbol{\kappa}, \qquad (6)$$

where s is process A, B, C, or D, and $\Delta_{\boldsymbol{\kappa}\alpha,hp,s}$ is the population change of hp phonons during process s involving phonon $\boldsymbol{\kappa}\alpha$ (1 or -1). The creation rate is estimated by integrating the interaction rate when $\Delta_{\boldsymbol{\kappa}\alpha,hp,s} = 1$ (for phonon hp annihilation, $\Delta_{\boldsymbol{\kappa}\alpha,hp,s} = -1$), and the net change in hp results from upconversion of low-energy acoustic phonons and downconversion to two acoustic phonons. Under equilibrium, the net population change of the LO, TO1 or TO2 is zero (based on the principle of detailed balance [26]), although the creation and annihilation rates are nonzero (e.g., $\dot{n}_{\text{LO},cr} = \dot{n}_{\text{LO},an} = 5.77 \times 10^{-8}$ s^{-1} per primitive cell at 300 K), and the net creation needs a nonequilibrium distribution with underpopulation of a targeted mode or overpopulation of other modes.
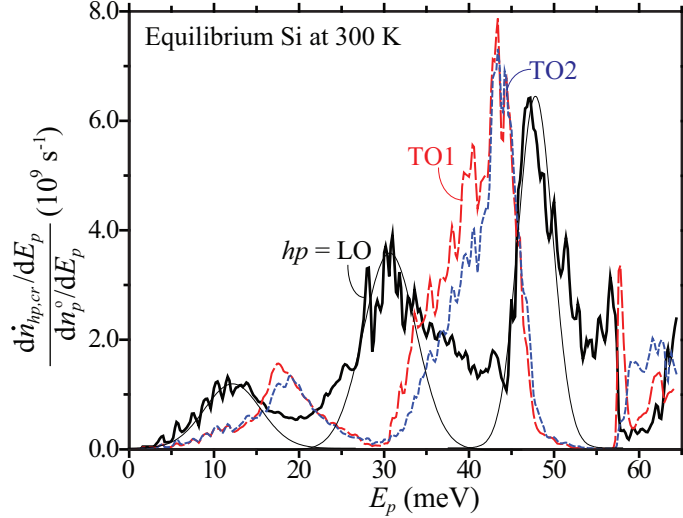
FIG. 2. Si optical-phonon creation rates in interaction with equilibrium phonon of energy E_p, at 300 K (for created phonons $hp = $ LO, TO1 and TO2). The rates (per unit time per unit energy in a primitive cell) are normalized using the equilibrium population distribution $\mathrm{d}n_p^\circ/\mathrm{d}E_p$.

To identify phonons most effective for upconversion, the spectral contribution to phonon creation/annihilation rates for hp are calculated by the projection of the rates for phonons with energy E_p, and shown in Fig. 2 under equilibrium at 300 K. Since the spectral contribution $\mathrm{d}\dot{n}_{hp,cr(\text{or } an)}/\mathrm{d}E_p$ is larger at energy with larger population, we normalize it with

population distribution $(\mathrm{d}n_p^\mathrm{o}/\mathrm{d}E_p)$ to identify single phonon contribution. Under equilibrium, the creation and annihilation are balanced, so only the creation rate is shown in Fig. 2. The results suggest that when overpopulated, the 12, 30, and 48 meV phonons are effective in LO phonon creation and the 19, 40 and 44 meV phonons are in TO phonon (results for TO1 and TO2 phonons are similar). The creation of these overpopulations is discussed next with the introduction of heterojunction phonon upconverter (HPUC).

III.   NONEQUILIBRIUM POPULATION

As discussed, the overpopulation of low-energy phonons [or underpopulation of high-energy (optical) phonons] is required for the net upconversion, and careful selection of these overpopulated modes leads to optimal conversion to targeted phonons. Although nonequilibrium occupancies $(f_p \neq f_p^\mathrm{o})$ are formed under the energy conversion and transport, these population deviations are not significant unless there is a transport with large temperature gradient or a high-energy injection in a short time [27]. To control distinct phonon nonequilibria, we introduce heterojunction where the contrast (mismatch) of phonon states results in junction (interface) reflections and local nonequilibria in the interfacial regions (although semiclassical treatments of interfacial phonon transport simply assume equilibrium, as discussed in [28, 29]).

With a given atomic density, a soft solid with lower Debye temperature has a larger population of low-energy phonons compared to a hard one (including its optical modes). Thus, in phonon transport from soft to hard material, the upconversion-favorable, low-energy phonon modes are more populated in the adjacent hard layer compared to the phonon transport in a homogeneous hard solid. We employ Ge as a soft semiconductor solid and Si as a hard one, and study the phonon transport across Ge/Si bilayer and the transported phonon harvesting (absorption) in Si in an energy conversion process.

For Ge/Si heterostructure the phonon properties and the upconversion processes are depicted in Fig. 3(a). With the same atomic structure (diamond cubic) and similar lattice constants (Ge: 5.65; Si: 5.43 Å) [30], their phonon dispersion and density of states $(D_{p,\mathrm{Ge}}$ and $D_{p,\mathrm{Si}})$ are similar with six phonon modes (the transverse modes are degenerated in Γ-X). However, the larger atomic mass and weaker interatomic force field result in larger population of low-energy phonons in Ge. Under phonon flux q_p (temperature gradient), the Ge phonons

7
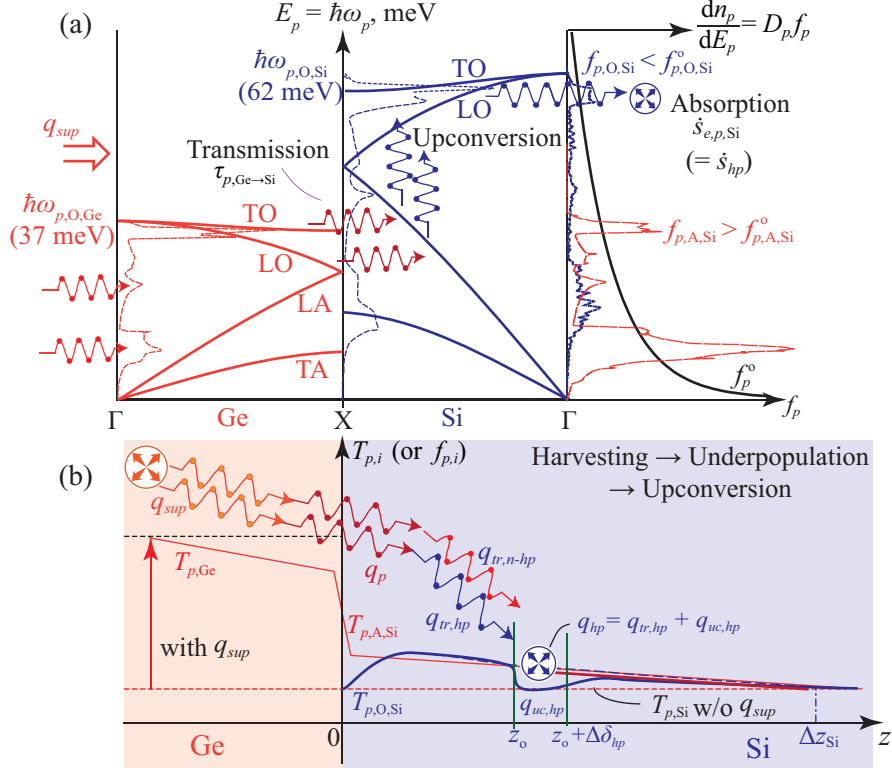
FIG. 3. Schematics of phonon harvesting in Ge/Si heterojunction (HPUC) (a) Phonon dispersion, density of states (D_p), and population distribution for Ge and Si. Under a flux, due to larger D_p at Ge acoustic and optical modes, the low-energy phonons in Si are overpopulated and then upconverted to Si-optical phonons. (b) Anticipated spatial distributions of the optical and acoustic-phonon temperatures ($T_{p,O}$ and $T_{p,A}$ with an interfacial temperature drop due to boundary resistance). The phonon source is in Ge and the phonon flux in z direction creates the temperature variations in Si. The Si-optical mode is less populated, because none is transmitted from Ge. The targeted phonon mode (hp) is harvested (absorbed by other system) in $[z_o, z_o + \Delta\delta_{hp}]$, and it leads to the underpopulation. The harvested phonon flux q_{hp} is due to transport of harvested ($q_{tr,hp}$) and conversion of nonharvested (n-hp) mode phonons ($q_{up,hp}$).

across the heterojunction create overpopulation of low-energy acoustic Si phonons (Ge, i.e., transmitted phonons) near the interface. These overpopulated phonons are upconverted to Si optical modes and harvested (otherwise downconverted by thermalization).

Phonons in Ge and Si are relaxed within a few hundred nm [31] from the interface, and also any atomic restructuring in the interfacial region does not extend beyond a few nm [29, 32]. So, over a distance of $O(100 \text{ nm})$ from the interface the phonons are relaxed to the equilibrium occupancy. Under thermal energy flux q_p, phonon temperature T_p (or population

8

f_p) increases compared to the initial equilibrium temperature, with the temperature gradient (spatial distribution of phonon population) depending on the transport property. With the large thermal conductivity of Ge and Si ($k_{\mathrm{Ge}} = 60$ and $k_{\mathrm{Si}} = 148$ W/m-K at 300 K [33]) and their interfacial phonon conductance ($G_{b,\mathrm{Ge/Si}}/A = 0.75$ GW/m²-K [31]), unless the phonon flux is extremely high (> 7.67 kW/cm²), the temperature variation over a distance of $O(100$ nm) on both sides of the interface, is negligible (< 1 K, within 1 μm interfacial region) [using the total thermal resistance ($AR_{\mathrm{Ge/Si}} = AR_{k,\mathrm{Ge}} + AR_{b,\mathrm{Ge/Si}} + AR_{k,\mathrm{Si}} = l/k_{\mathrm{Ge}} + A/G_{b,\mathrm{Ge/Si}} + l/k_{\mathrm{Si}} = 130$ μK-cm²/W, where $l = 0.5\mu$m)]. We consider heterojunction upconversion within a length of $O(100$ nm) from the interface and a phonon flux less than 7.67 kW/cm², so the temperature change over the interested heterostructure region is negligible. The phonon population change due to this heat flux is not significant after relaxation, and the phonons upstream (before transmission across the heterojunction) are assumed to be in equilibrium.

With phonon flux from the Ge layer, the spatial distributions of the anticipated optical and acoustic phonon temperatures in the HPUC system are shown in Fig. 3(b). Since the Ge-transmitted phonons are not populated in the Si-optical mode range, the optical temperature at the interface is not increased by the phonon flux. However, as the transmitted acoustic phonons are upconverted (relaxed), the optical phonon temperature follows the acoustic counterpart. If we harvest optical phonons (absorbed by other system) in $[z_o, z_o + \Delta\delta_{hp}]$ ($\Delta\delta_{hp}$ is the length of phonon-harvesting region), the harvested phonon mode (hp) is underpopulated (lower phonon temperature) and enhances the upconversion. Thus, the harvested (or absorbed) phonons can be supplied by the conversion of nonharvested (n-hp) mode as well as the transport of harvested mode (hp) phonons (created between the interface and the harvested site).

The equilibrium population distributions are calculated using the equilibrium occupancy function f_p^o and the phonon density of states D_p calculated from the DFPT, i.e. $\mathrm{d}n_p^o/\mathrm{d}E_p = D_p f_p^o$, and the results for Ge and Si are shown in Fig. 4(a) for 300 K. To predict the distribution of the Ge/Si heterojunction transmitted phonons, the spectral phonon junction transmission from Ge to Si $\tau_{p,\mathrm{Ge}\to\mathrm{Si}}(E_p)$ and the Ge equilibrium distribution $\mathrm{d}n_{p,\mathrm{Ge}}^o/\mathrm{d}E_p$ are used. The transmitted distribution in the Si layer is estimated as $\mathrm{d}n_p/\mathrm{d}E_p|_{z=+0} = \tau_{p,\mathrm{Ge}\to\mathrm{Si}}\mathrm{d}n_{p,\mathrm{Ge}}^o/\mathrm{d}E_p$ (interface at $z = 0$), and these phonons originating from the Ge layer is named as the Ge-transmitted phonons compared with the Si-native phonons.

The nonequilibrium Green function (NEGF) formalism [35] provides the spectral trans-

mission used in the prediction of nonequilibrium phonon distribution. In NEGF calculations, the interface is a scattering region, with the two sides having equilibrium populations away from this interface (reservoirs not affected by the transport). The phonon transmission across the interface represents scattering by the interfacial-region structure, and the transmitted phonons will be further relaxed through the p-p interactions. All the functions required in the NEGF are calculated using the force-constant matrices of the heterojunction. Among them, the self-energy ($\mathbf{\Sigma}_L^r$ or $\mathbf{\Sigma}_R^r$, where superscript r represents retarded as opposed to advanced (a), and subscripts L and R represent left and right) represents the interaction of semi-infinite Ge and Si layers (slabs) with the heterojunction, and is calculated employing the decimation technique [36]. Using the self-energy, the phonon retarded Green function is given by [37]

$$\mathbf{G}^r = [(\omega + i\eta)^2 \mathbf{I} - \mathbf{K}_{CC} - \mathbf{\Sigma}_L^r - \mathbf{\Sigma}_R^r], \tag{7}$$

where $\mathbf{I}$ is the identical matrix, $\mathbf{K}_{CC}$ is the force constant matrix of the heterojunction at center, ω is the angular frequency of phonon, and η is an infinitesimal number for the phonon
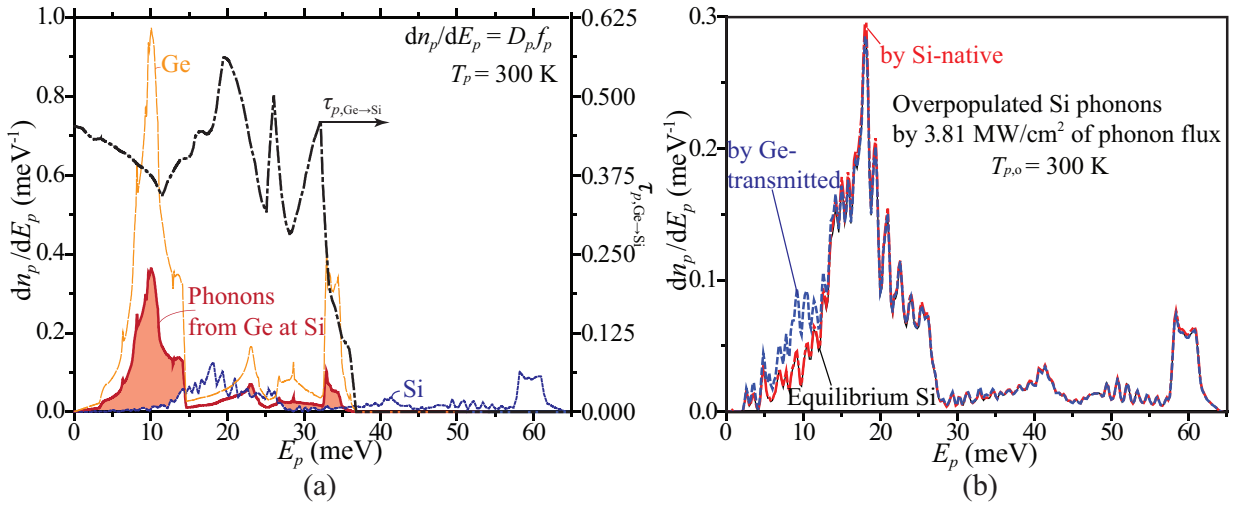
FIG. 4. (a) Phonon population (per primitive cell) distributions adjacent to junction, based on the NEGF transmission spectrum [34] for the Ge/Si phonons (right axis), at 300 K. Shaded regions represent larger overpopulation by transmitted Ge phonons. The Si and Ge equilibrium distributions are also shown for contrast. (b) Nonequilibrium phonon distribution created by the Ge-transmitted and the Si-native phonons under the same phonon flux (3.8 MW/cm^2). The Si phonon modes matching the Ge phonons are more pronouncedly overpopulated by the Ge-transmitted phonon flux.

10

energy dissipation [38]. Then, the phonon transmission across the heterojunction is [39, 40]

$$\tau_p = \mathrm{Tr}[\boldsymbol{\Gamma}_L \boldsymbol{G}^r \boldsymbol{\Gamma}_R \boldsymbol{G}^a], \tag{8}$$

where $\boldsymbol{G}^a$ is the phonon advanced Green function equivalent to $(\boldsymbol{G}^r)^\dagger$ and $\boldsymbol{\Gamma}_L(\boldsymbol{\Gamma}_R)$ is the energy-level broadening function caused by the left (right) contact and described by $\boldsymbol{\Gamma}_{L/R} = i(\boldsymbol{\Sigma}_{L/R}^r - \boldsymbol{\Sigma}_{L/R}^a)$.

We employed the NEGF spectral transmission [using the right axis in Fig. 4(a)] of the Ge/Si heterojunction from Ref. [34], where the force constant matrices are calculated using the many-body Tersoff potential [41] and an ideal (perfectly smooth) interface is assumed. (The results from Ref. [34] agree well with other reports [42, 43].) The atomic roughness affects the interfacial phonon scattering depending on the phonon wavelength (or frequency) and the incident angle [42]. Depending on the atomic configuration, well-controlled roughness can increase the transmission (especially at midrange frequency) by smoothening the abrupt acoustic impedance mismatch and increase in interfacial area [44]. Thus, nonequilibrium phonon distribution can be further tuned using the interfacial atomic roughness. Also, since the harmonic (second-order) force constants are used in the Green function calculation, the anharmonic effects are excluded in this transmission (anharmonicity can be included in NEGF [45]).

The transmitted Ge-phonon distribution at the Si-side interface calculated using the NEGF transmission is shown in Fig. 4(a), and its occupancy in Si is nonequilibrium ($f_{p,\mathrm{Ge/Si}} = \tau_{p,\mathrm{Ge}\to\mathrm{Si}} D_{p,\mathrm{Ge}} f_p^\mathrm{o}/D_{p,\mathrm{Si}}$, where subscript Ge/Si is for Ge-transmitted phonons in Si). Through this heterojunction transport with nonunity spectral transmission, Si phonons in ranges of [0, 14.5 meV] and [26, 35 meV] are overpopulated, and these phonons are effective to create Si LO phonons according to the results shown in Fig. 2. The phonons, transported from Ge to Si, eventually relax to Si phonon equilibrium population, but the transported phonon distribution remains deviated from equilibrium until fully relaxed, and this deviation is the most prominent adjacent to the interface. In particular, those Si phonon modes matching the Ge phonons are pronouncedly more overpopulated compared to equilibrium population.

The transmitted Ge phonons are added to the equilibrium population of Si, and this nonequilibrium contribution increases with the phonon flux q_p. In addition, we impose optical phonon harvesting in the Si layer, and this is done by maintaining the population of

11

Si optical phonons. For steady, phonon harvesting, we balance the Si optical phonons created by the Ge phonon transmission with the harvesting (absorption) of these Si optical phonons, so here the population of the harvested phonons (hp) is assumed to be in equilibrium, while allowing for the overpopulation of the Ge-transmitted modes. The non-harvested (n-hp, acoustic in Si) modes are overpopulated by the transmitted phonons ($f_{p,\kappa\alpha} > f^o_{p,\kappa\alpha}$), and this nonequilibrium phonons in transit contribute to the phonon flux as [3]

$$q_p = \frac{1}{8\pi^3} \sum_{\alpha} \int_{\mathrm{BZ}} f'_{p,\kappa\alpha} u_{p,\kappa\alpha} \hbar\omega_{p,\kappa\alpha} \mathrm{d}\kappa, \tag{9}$$

where $f'_{p,\kappa\alpha}$ is the occupancy deviation from equilibrium of phonon $\kappa\alpha$ ($f_{p,\kappa\alpha} - f^o_{p,\kappa\alpha}$), and $u_{p,\kappa\alpha}$ is the phonon velocity. Here, the deviation originates from the overpopulated phonons propagating in the transport direction ($f'_{p,\kappa\alpha} = f^+_{p,\kappa\alpha}$).

To study the upconversion effectiveness of the HPUC structure, the overpopulation distributions by the Ge-transmitted (across the Ge/Si heterojunction) and the Si-native phonon fluxes, are considered, and the former is only observed near the interface in the Si layer, while the latter persists sufficiently far from the interface. The overpopulated phonon populations are estimated as a fraction of the Ge-transmitted phonons and equilibrium Si-phonons in Fig. 4(a); i.e., $f^+_p = af_{p,\mathrm{Ge/Si}}$ and $bf^o_{p,\mathrm{Si}}$ with a and b as constants, where subscripts Ge/Si and Si are for the Ge-transmitted and Si-native, respectively. The overpopulated energy in primitive cell is $\langle E^+_p \rangle = \int D_p f^+_p \mathrm{d}E_p$, and using Eq. (9) and the spectral mode-average velocities from Ref. [46], we have $q_p = (1.27 \ \mathrm{kW/cm^2}\text{-}\mu\mathrm{eV})\langle E^+_{p,\mathrm{Ge/Si}} \rangle$, where $\langle E^+_{p,\mathrm{Ge/Si}} \rangle$ is the overpopulated the Ge-transmitted phonon energy in primitive cell. The native-Si phonon overpopulation $\langle E^+_{p,\mathrm{Si}} \rangle$ with the same q_p is used as the benchmark. Since high-speed, low-energy phonons are less populated in the Si-native phonons than the Ge-transmitted, $\langle E^+_{p,\mathrm{Si}} \rangle$ is larger than $\langle E^+_{p,\mathrm{Ge/Si}} \rangle$ for the same q_p.

The nonequilibrium (NE) population distribution is $\mathrm{d}n_p/\mathrm{d}E_p = D_p(f^o_{p,\mathrm{Si}} + f^+_p)$, while the harvested-mode population remains at equilibrium. Figure 4(b) shows the transmission-induced population increase and deviation from the equilibrium distribution. We also show the imposed uniform overpopulation of the Si-native phonon used in the phonon upconversion under the same phonon flux. Here the overpopulation is added to the Si equilibrium phonon distribution ($f^o_{p,\mathrm{Si}}$) at 300 K. For more a pronounced deviation, the overpopulated distributions under very high phonon flux of 3.8 MW/cm^2 (which induces 3 meV overpopulation per primitive cell for the Ge-transmitted phonons) are shown in Fig. 4(b).

This nonequilibrium can be observed by measuring the phonon optical properties or analyzing the atomic vibration simulations such as *ab initio* or classical molecular dynamics. The Ge phonons transmitted to Si layer, i.e., undergoing filtering, change the local phonon population in Si and this can be measured to confirm the nonequilibrium population a short distance from the interface. Phonons, having large momentum and relatively small energy, assist in the photon-matter interactions [47, 48], so the larger phonon population, the larger the photon absorption/emission rate [49]. The nonequilibrium phonons are also observed with the X-ray methods, e.g., the X-ray scattering which is sensitive to the short-wavelength phonons which reduce the intensity of the Bragg peaks and produce diffuse scattering background [50]. Also, the time-resolved anti-Stokes Raman (ASR) scattering can measure the population change [51–53]. In addition to experiments, the change in the phonon population distribution can be simulated with molecular dynamics (classical [54] and *ab initio* [55]) and analysis of the local, atomic displacements.

IV. UPCONVERSION EFFICIENCY

Under nonequilibrium (NE), the optical-mode creation and annihilation rates are no longer balanced. Using the nonequilibrium distributions by the Ge-transmitted and the Si-native phonon fluxes for the heat flux $q_p = 1.27$ kW/cm^2, where $\langle E_{p,\text{Si}}^+ \rangle = 1.24$ μeV and $\langle E_{p,\text{Ge/Si}}^+ \rangle = 1$ μeV) (for this overpopulation, $a = 3.01 \times 10^{-5}$ and $b = 2.31 \times 10^{-5}$ in $f_p^+ = a f_{p,\text{Ge/Si}}$ and $b f_{p,\text{Si}}^o$), the net creation rate for the targeted (harvested) phonon hp is calculated using Eq. (6). When the Si LO-mode phonons are harvested ($hp = \text{LO}$), the net creation rates by the Si-native and the Ge-transmitted phonons are $\dot{s}_{\text{LO,Si}} = 1.43$ W/cm^2-nm, and $\dot{s}_{\text{LO,Ge/Si}} = 1.33$ W/cm^2-nm. The net creation rate (mainly by upconversion) increases with increase in q_p (f_p^+ or $\langle E_p^+ \rangle$), and for $q_p < 1$ MW/cm^2, the hp-phonon energy generation rate $\dot{s}_{hp}$ is linearly proportional to q_p. Since both the Ge-transmitted and Si-native overpopulations are added to the same equilibrium, the spatial temperature variations should be minimized to ignore the variation of equilibrium distribution, and for $q_p < 7.67$ kW/cm^2 in the linear regime of the q_p-$\dot{s}_{hp}$ relation, we find variation $\Delta T < 1$ K within 1 μm of the junction region. So, under the linear relation and small T-variation limit, we normalize $\dot{s}_{hp}$ with heat flux q_p and average phonon mean free path λ_p, i.e., $\dot{s}_{hp}^* = \dot{s}_{hp}/(q_p/\lambda_p)$. The phonon mean free path ($\lambda_p = 115$ nm) is estimated from the phonon transport properties

13

using the conductivity relation $k_p = nc_v u_p \lambda_p / 3$, where n is phonon number density, c_v is specific heat capacity, and the spectral mode-average velocities from Ref. [46] are used for phonon velocity u_p [3, 30]. This gives $\dot{s}^*_{\mathrm{LO,Si}} = 0.127$ and $\dot{s}^*_{\mathrm{LO,Ge/Si}} = 0.121$ at 300 K. For the upconversion to TO1 and TO2 modes, $\dot{s}^*_{\mathrm{TO1,Si}} = 0.173$ and $\dot{s}^*_{\mathrm{TO1,Ge/Si}} = 0.0696$, and $\dot{s}^*_{\mathrm{TO2,Si}} = 0.159$ and $\dot{s}^*_{\mathrm{TO2,Ge/Si}} = 0.0545$. For all three optical modes, the net creation rate by Si-native overpopulated phonons ($f_p^+ = b f_{p,\mathrm{Si}}^o$) is larger than the NE Ge-transmitted phonons ($f_p^+ = a f_{p,\mathrm{Ge/Si}}$) with the same heat flux, and the difference between these two is the smallest for the LO-mode upconversion. The $a f_{p,\mathrm{Ge/Si}}$ is expected to favor the LO-mode upconversion from Figs. 2 and 4, and these results confirm this.

Depending on phonon-harvesting system, different phonon wavevectors are required [56], so we study the upconversion to optical phonons with the selected wavevectors. We sample the grid ($V_{\mathrm{BZ}}/19683$, V_{BZ}: first BZ) and the dimensionless, local net creation rate for the phonon $\boldsymbol{\kappa}^* \alpha$ per dimensionless reciprocal volume ($\mathrm{d}\dot{s}^*_{\boldsymbol{\kappa}\alpha}/\mathrm{d}\boldsymbol{\kappa}^*$ for $hp = \boldsymbol{\kappa}^* \alpha$) is calculated with respect to dimensionless wavevector $\boldsymbol{\kappa}^*$ (normalized by $2\pi/a$, a: lattice constant) with one optical mode ($\mathrm{d}\dot{s}^*_{\boldsymbol{\kappa}\alpha}/\mathrm{d}\boldsymbol{\kappa}^* = 0$ under equilibrium). We integrate this rate for selected wavevector space ($\boldsymbol{\kappa}^* = \boldsymbol{\kappa}^*_{\mathrm{sel}}$), i.e., $\dot{s}^*_{(\boldsymbol{\kappa}^*=\boldsymbol{\kappa}^*_{\mathrm{sel}})\alpha} = \int_{\boldsymbol{\kappa}^*=\boldsymbol{\kappa}^*_{\mathrm{sel}}} (\mathrm{d}\dot{s}^*_{\boldsymbol{\kappa}\alpha}/\mathrm{d}\boldsymbol{\kappa}^*)\mathrm{d}\boldsymbol{\kappa}^*$.

The dimensionless, local net creation rate for LO phonons ($\alpha = \mathrm{LO}$) is calculated on irreducible $\boldsymbol{\kappa}$-points in $27 \times 27 \times 27$ sampling grid for NE Si-native and NE Ge-transmitted prescribed overpopulations, and are plotted along high-symmetry axes in Fig 5(a). The difference between these two rates is also plotted in one irreducible BZ wedge in Fig. 5(b). Both figures show that overall NE Ge-transmitted phonons have smaller $\mathrm{d}\dot{s}^*_{\boldsymbol{\kappa}\alpha}/\mathrm{d}\boldsymbol{\kappa}^*$ when creating LO phonons near Γ [i.e. $\boldsymbol{\kappa}^* = (0,0,0)$], compared to NE Si-native phonons. In addition to the zone center region (Γ), NE Si-native phonons are more effectively upconverted to LO phonons in the zone boundary $\boldsymbol{\kappa}^*$ points around the U-W-K line, while NE Ge-transmitted phonons are effective for harvesting the LO phonons near the L or X points. The Ge-transmitted phonons provide large population around 10 and 33 meV [Fig. 4(a)], interact with equilibrium (E) Si phonons (peaks near 18 and 42 meV), and effectively upconvert to Si-LO phonons between 49 and 56 meV [especially 51 (33+18) and 52 (10+42) meV] [Fig. 5(a)].

In upconverted optical-phonon harvesting, the efficiency η_{hp} is defined as the ratio of harvested q_{hp} to supplied q_{sup} phonon fluxes (in Ge), $\eta_{hp} = q_{hp}/q_{sup}$, and this includes the junction transmission and upconversion processes. With the heterojunction, q_{sup} in the
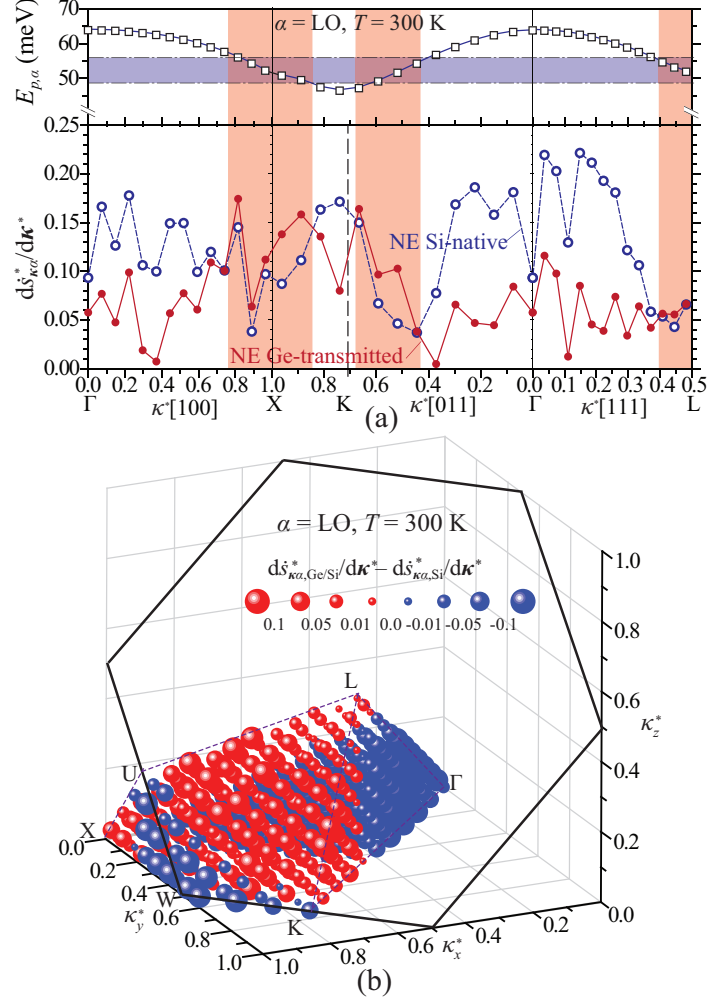
FIG. 5. (a) Variations of dimensionless, local net creation (upconversion) rates for LO phonons ($\mathrm{d}\dot{s}^*_{\boldsymbol{\kappa}\alpha}/\mathrm{d}\boldsymbol{\kappa}^*$; $\alpha = \mathrm{LO}$) from Ge-transmitted and Si-native overpopulated phonons, along high-symmetry axes. The created optical-phonon energy ($E_{p,\mathrm{LO}}$) is also shown (upper), and it is evident that overpopulation by the Ge-transmitted phonons results in larger LO phonon creation rate in regime [49, 56 meV] compared to the NE Si-native phonons. (b) Difference between $\mathrm{d}\dot{s}^*_{\boldsymbol{\kappa}\alpha,\mathrm{Si}}/\mathrm{d}\boldsymbol{\kappa}^*$ and $\mathrm{d}\dot{s}^*_{\boldsymbol{\kappa}\alpha,\mathrm{Ge/Si}}/\mathrm{d}\boldsymbol{\kappa}^*$ in an irreducible BZ wedge. Spheres are centered at the sampling points of $27 \times 27 \times 27$ grid, showing the wavevector of upconverted (harvested) phonon. Red represents larger $\mathrm{d}\dot{s}^*_{\boldsymbol{\kappa}\alpha,\mathrm{Ge/Si}}/\mathrm{d}\boldsymbol{\kappa}^*$ and blue larger $\mathrm{d}\dot{s}^*_{\boldsymbol{\kappa}\alpha,\mathrm{Si}}/\mathrm{d}\boldsymbol{\kappa}^*$, and diameter indicates the magnitude. The results are for 300 K.

ballistic regime is predicted from the transmission $\tau_{p,\mathrm{Ge}\to\mathrm{Si}}$ and actual phonon flux over the system q_p, and considering the transmission and phonon flux depending on the wavevector and mode, $q_{sup} = \sum_\alpha \int_{\mathrm{BZ}} (\mathrm{d}q_{sup,\boldsymbol{\kappa}\alpha}/\mathrm{d}\boldsymbol{\kappa}^*)\mathrm{d}\boldsymbol{\kappa}^* = \sum_\alpha \int_{\mathrm{BZ}} \mathrm{d}q_{p,\boldsymbol{\kappa}}/(\tau_{p,\boldsymbol{\kappa}\alpha,\mathrm{Ge}\to\mathrm{Si}}\mathrm{d}\boldsymbol{\kappa}^*)\mathrm{d}\boldsymbol{\kappa}^*$, where $\mathrm{d}q_{sup(\mathrm{or}\ p),\boldsymbol{\kappa}\alpha}/\mathrm{d}\boldsymbol{\kappa}^*$ is the contribution of phonon $\boldsymbol{\kappa}^*\alpha$ to the heat flux $q_{sup(\mathrm{or}\ p)}$ (heat flux by

15

phonon $\boldsymbol{\kappa}^*\alpha$ per dimensionless reciprocal volume), and $\mathrm{d}q_{p,\boldsymbol{\kappa}\alpha}/\mathrm{d}\boldsymbol{\kappa}^* = \tau_{p,\boldsymbol{\kappa}\alpha,\mathrm{Ge}\to\mathrm{Si}}(\mathrm{d}q_{sup,\boldsymbol{\kappa}\alpha}/\mathrm{d}\boldsymbol{\kappa}^*)$ in the ballistic regime. Under steady state, the harvested phonon flux q_{hp} is balanced with transported, harvested optical-phonon flux $q_{tr,hp}$ [using Eq. (9) for hp mode] and the upconverted phonon flux $q_{uc,hp}$; thus, $q_{hp} = q_{tr,hp} + q_{uc,hp}$. The latter is the integration of the upconversion rate over the phonon-harvesting region $\Delta\delta_{hp}$ [in Fig. 2(b)], i.e.,

$$q_{uc,hp} = \int_{\Delta\delta_{hp}} \dot{s}_{hp}\mathrm{d}z.$$

Since the phonon flux from Ge does not include optical modes (i.e., there is no transported, harvested phonon, $q_{tr,hp}$) and with the nonunity junction transmission further reducing the flux, low efficiency is expected for the NE Ge-transmitted phonons. This holds even for the Ge-favored upconversion channels (i.e., resulting in $\mathrm{d}\dot{s}^*_{\boldsymbol{\kappa}\alpha,\mathrm{Ge/Si}}/\mathrm{d}\boldsymbol{\kappa}^* > \mathrm{d}\dot{s}^*_{\boldsymbol{\kappa}\alpha,\mathrm{Si}}/\mathrm{d}\boldsymbol{\kappa}^*$). As the transported phonon distribution evolves from the NE Ge-transmitted to NE Si-native through the relaxation, the phonon flux includes the harvested mode ($q_{tr,hp}$) and the upconversion rate becomes close to the NE Si-native $\dot{s}_{\boldsymbol{\kappa}\alpha,\mathrm{Si}}$.

We calculate the spatial (from the junction) variations of efficiency at selected $\boldsymbol{\kappa}^*$ points with $\Delta z = \lambda_p/10$ of harvesting bins ($\Delta\delta_{hp} = \Delta z$). The overpopulation distribution in $0 \leq z \leq \lambda_p$ is treated as linear interpolation of Ge-transmitted and Si-native overpopulations, and
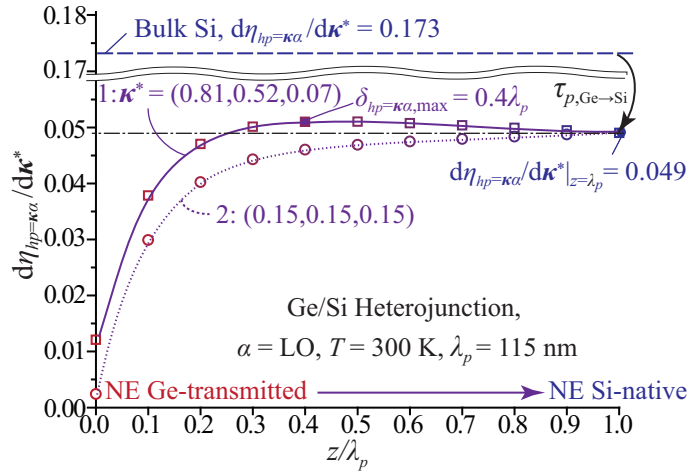
FIG. 6. Spatial variations of the local harvesting efficiency ($\mathrm{d}\eta_{hp=\boldsymbol{\kappa}\alpha}/\mathrm{d}\boldsymbol{\kappa}^*$) for two wavevectors, $\boldsymbol{\kappa}^* = (0.81, 0.52, 0.07)$ near zone boundary (solid), and $(0.15, 0.15, 0.15)$ near zone center (dotted). For the first, an optimal location for efficiency (filled square) exists before relaxation, while for the second the efficiency increases monotonically. $\mathrm{d}\eta_{hp=\boldsymbol{\kappa}\alpha}/\mathrm{d}\boldsymbol{\kappa}^*$ in bulk Si (dashed) is larger with no loss by heterojunction transmission ($\tau_{p,\mathrm{Ge}\to\mathrm{Si}}$).

the transported $\boldsymbol{\kappa}^*\alpha$ phonon flux $q_{tr,\boldsymbol{\kappa}\alpha}$ and creation rate $\dot{s}_{\boldsymbol{\kappa}\alpha}$ (for selected $hp = \boldsymbol{\kappa}^*\alpha$) follow this variation. Adding the low velocity and short lifetime of the optical phonons (shorter relaxation length), $q_{tr,\boldsymbol{\kappa}\alpha}$ approaches NE Si-native magnitude faster than upconverted $\boldsymbol{\kappa}^*\alpha$ phonon flux $q_{uc,\boldsymbol{\kappa}\alpha}$ (and $\dot{s}_{\boldsymbol{\kappa}\alpha}$).

Figure 6 shows variation of local harvesting efficiency $\mathrm{d}\eta_{hp=\boldsymbol{\kappa}\alpha}/\mathrm{d}\boldsymbol{\kappa}^*$ (using $q_{\boldsymbol{\kappa}\alpha}$ per dimensionless reciprocal volume) for two $\boldsymbol{\kappa}^*\alpha$; 1. $\alpha = \mathrm{LO}$ and $\boldsymbol{\kappa}^* = (0.81, 0.52, 0.07)$, which is more effectively upconverted by the Ge-transmitted compare to the Si-native phonons, $\mathrm{d}\dot{s}^*_{\boldsymbol{\kappa}\alpha,\mathrm{Ge/Si}}/\mathrm{d}\boldsymbol{\kappa}^* > \mathrm{d}\dot{s}^*_{\boldsymbol{\kappa}\alpha,\mathrm{Si}}/\mathrm{d}\boldsymbol{\kappa}^*$, and 2. $\alpha = \mathrm{LO}$ and $\boldsymbol{\kappa}^* = (0.15, 0.15, 0.15)$ where $\mathrm{d}\dot{s}^*_{\boldsymbol{\kappa}\alpha,\mathrm{Ge/Si}}/\mathrm{d}\boldsymbol{\kappa}^* < \mathrm{d}\dot{s}^*_{\boldsymbol{\kappa}\alpha,\mathrm{Si}}/\mathrm{d}\boldsymbol{\kappa}^*$. For the first $\boldsymbol{\kappa}^*$, an optimal (not that pronounced) location for harvesting ($\delta_{hp=\boldsymbol{\kappa}\alpha,\mathrm{max}}$) exists before the relaxation. For the second $\boldsymbol{\kappa}^*$, both $q_{tr,\boldsymbol{\kappa}\alpha}$ and $q_{uc,\boldsymbol{\kappa}\alpha}$ increase as the flux is relaxed and the local harvesting efficiency $\mathrm{d}\eta_{hp=\boldsymbol{\kappa}\alpha}/\mathrm{d}\boldsymbol{\kappa}^*$ increases monotonically. So, depending on the $q_{tr,\boldsymbol{\kappa}\alpha}$ variation, which can dominate over variation of $q_{uc,\boldsymbol{\kappa}\alpha}$, $\delta_{hp=\boldsymbol{\kappa}\alpha,\mathrm{max}}$ can be larger than λ_p. The bulk Si and the fully relaxed region in Ge/Si ($z > \lambda_p$) have the same overpopulation and $q_{\boldsymbol{\kappa}\alpha}$ with a given q_p, but in bulk Si q_{sup} is smaller by $\tau_{p,\mathrm{Ge}\rightarrow\mathrm{Si}}$ and $\mathrm{d}\eta_{hp=\boldsymbol{\kappa}\alpha}/\mathrm{d}\boldsymbol{\kappa}^*$ is larger than Ge/Si structure as shown in Fig. 6. Thus, compared to native phonons in bulk Si, the overall harvesting efficiency η_{hp} for the transmitted phonons is smaller, because of the interfacial reflection, even though the upconversion efficiency excluding the phonon supply by transport i.e., $\eta_{uc,hp} = q_{uc,hp}/q_{sup}$, is larger for the NE Ge-transmitted phonons. As the phonons are harvested and the phonon flux is reduced (the harvesting site is located adjacent to the interface and within the relaxation length), this phonon flux reduction depends on the phonon flow direction (i.e., flowing from the soft to hard solid, or vice versa). This is due to distinct NE phonon populations of two sides. This direction dependency is a thermal rectification [57] and its magnitude depends on the harvested phonon mode and location, as shown in Fig. 6.

V. CONCLUSIONS

In quest for increase in the solid-state energy conversion efficiency, resonant phonons may be targeted for harvesting instead of heat (equilibrium phonon occupancy). These nonequilibrium phonons may be available as a result of local emission (including nonradiative decay), but may also be created by phonon-phonon interactions. For the effective supply of the energetic optical (resonant) phonons, the p-p interaction kinetics and the nonequilibrium phonon

17

distribution are controlled by the heterojuction transmission. Here we have compared the effectiveness of nonequilibrium native and the heterojunction (soft/hard bilayer) transmitted phonons for upconversion to optical phonons, addressed the related phonon physics and interaction kinetics, defined upconversion efficiency, and made specific calculations for the Ge/Si bilayer. The creation and annihilation rates of the Si optical phonons are calculated using the third-order force constants from DFPT, and the effective phonons for creating the targeted optical modes are identified (the 12, 30, and 48 meV phonons for LO phonon creation and the 19, 40 and 44 meV phonons for TO phonon). The nonequilibrium distribution by the heterojunction transmitted phonons is estimated using the spectral transmission (from NEGF), and it is shown that the Ge-transmitted phonons create large populations of the low-energy acoustic and the Ge optical mode, which are effective in the creation of the Si LO (for harvesting absorption). The nonequilibrium Ge-transmitted and the Si-native phonons have their distinct high upconversion efficiency regions in the Brillouin zone, which can be targeted for harvesting. For example, since Si is an indirect-gap semiconductor [valance band at and conduction band near the X point (multiple locations)], phonons near the zone boundary are harvested through the phonon-assisted, photon absorption processes [58]. Here we show that the Ge-transmitted phonons can also create/supply these phonons (the Ge-transmitted phonons are effective for the zone-boundary phonons near the L and X points, and the Si-native phonons for the other regions).

Substituting Ge by another soft solid, for example by InP, which has optical mode at 42 meV [59], can be more effective for the Si TO phonon creation, as suggested by Fig. 2. Also, using the alloy $Si_x Ge_{1-x}$, which has additional optical mode at 50 meV (for LO phonon creation), allows for the resonant, high-upconversion-efficiency selection by choosing a Si content x [60]. Energy conversion among the nonequilibrium phonon modes leads to fundamental improvements in the resonant phonon harvesting, including the thermal rectification which accompanies the phonon-flux-direction-dependent phonon harvesting, and the infrared photon emission through the absorption of optical phonons. Traditionally, phonons are regarded as energy dissipation agents or the parasite interferers with the electron transport; however with the control of the phonon population distribution and the related interaction kinetics, as suggested here, the harvesting of resonance phonons as energy source can evolve the phonon research and phononic applications [61, 62].

ACKNOWLEDGMENTS

[1] M. Lundstrom, *Fundamentals of Carrier Transport* (Cambridge University Press, New York, 2000).

[2] R. D. Mattuck and M. W. P. Strandberg, Phys. Rev. **119**, 1204 (1960).

[3] M. Kaviany, *Heat Transfer Physics*, 2nd ed. (Cambridge University Press, New York, 2014).

[4] G. P. Srivastava, *The Physics of Phonons* (Adam Hilger, Bristol, 1990).

[5] M. Haase and H. Schäfer, Angew. Chem. Int. Ed. **50**, 5808 (2011).

[6] F. Auzel, Chem. Rev. **104**, 139 (2003).

[7] H. U. Güdel, Chimia **52**, 561 (1998).

[8] S. Shin, C. Melnick, and M. Kaviany, Phys. Rev. B **87**, 075317 (2013).

[9] X. L. Ruan and M. Kaviany, Phys. Rev. B **73**, 155422 (2006).

[10] J. Kim and M. Kaviany, Phys. Rev. B **82**, 134205 (2010).

[11] K. Winer and M. Cardona, Phys. Rev. B **35**, 8189 (1987).

[12] G. Deinzer and D. Strauch, Phys. Rev. B **69**, 045205 (2004).

[13] J. E. Turney, E. S. Landry, A. J. H. McGaughey, and C. H. Amon, Phys. Rev. B **79**, 064301 (2009).

[14] S. Merabia and K. Termentzidis, Phys. Rev. B **86**, 094303 (2012).

[15] I. N. Adamenko, K. E. Nemchenko, A. V. Zhukov, M. A. H. Tucker, and A. F. G. Wyatt, Physica B **284-288**, 31 (2000).

[16] D. Vanderbilt, S. G. Louie, and M. L. Cohen, Phys. Rev. B **33**, 8740 (1986).

[17] D. J. Ecsedy and P. G. Klemens, Phys. Rev. B **15**, 5957 (1976).

[18] A. A. Maradudin and A. E. Fein, Phys. Rev. **128**, 2589 (1962).

[19] G. Deinzer, G. Birner, and D. Strauch, Phys. Rev. B **67**, 144304 (2003).

[20] O. Hellman and I. A. Abrikosov, Phys. Rev. B **88**, 144301 (2013).

[21] J. R. Yates, X. Wang, D. Vanderbilt, and I. Souza, Phys. Rev. B **75**, 195121 (2007).

[22] H. J. Monkhorst and J. D. Pack, Phys. Rev. B **13**, 5188 (1976).

[23] S. Baroni, S. de Gironcoli, A. Dal Corso, and P. Giannozzi, Rev. Mod. Phys. **73**, 515 (2001).

[24] X. Gonze and J.-P. Vigneron, Phys. Rev. B **39**, 13120 (1989).

[25] P. Giannozzi *et al.*, J. Phys.: Condens. Matter **21**, 395502 (2009).

[26] M. J. Klein, Phys. Rev. **97**, 1446 (1955).

[27] V. Spagnolo, M. S. Vitiello, G. Scamarcio, B. S. Williams, S. Kumar, Q. Hu, and J. L. Reno, J. Phys.: Conf. Ser. **92**, 012018 (2007).

[28] E. T. Swartz and R. O. Pohl, Rev. Mod. Phys. **61**, 605 (1989).

[29] S. Shin, M. Kaviany, T. Desai, and R. Bonner, Phys. Rev. B **82**, 081302 (2010).

[30] A. Dargys and J. Kundrotas, *Handbook on physical properties of* Ge, Si, GaAs *and* InP (Science and Encyclopedia Publishers).

[31] Y. Chalopin, K. Esfarjani, A. Henry, S. Volz, and G. Chen, Phys. Rev. B **85**, 195302 (2012).

[32] H. Hibino and T. Ogino, Phys. Rev. B **49**, 5765 (1994).

[33] W. M. Haynes (Editor), *CRC Handbook of Chemistry and Physics, 94th Edition* (CRC Press, 2013).

[34] X. Li and R. Yang, J. Phys.: Condens. Matter **24**, 155302 (2012).

[35] S. Shin and M. Kaviany, Phys. Rev. B **84**, 235433 (2011).

[36] M. P. Lopez Sancho, J. M. Lopez Sancho, and J. Rubio, J. Phys. F **15**, 851 (1985).

[37] J.-S. Wang, X. Ni, and J.-W. Jiang, Phys. Rev. B **80**, 224302 (2009).

[38] W. Zhang, T. S. Fisher, and N. Mingo, Numer. Heat Transfer, Part B **51**, 333 (2007).

[39] S. Datta, *Electronic Transport in Mesoscopic Systems* (Cambridge University Press, Cambridge, 1997).

[40] C. Caroli, R. Combescot, P. Nozieres, and D. Saint-James, J. Phys. C: Solid St. Phys. **4**, 916 (1971).

[41] J. Tersoff, Phys. Rev. B **39**, 5566(R) (1989).

[42] Z. T. Tian, K. Esfarjani, and G. Chen, Phys. Rev. B **86**, 235304 (2012).

[43] H. Zhao and J. B. Freund, J. Appl. Phys. **97**, 024903 (2005).

[44] S. Merabia and K. Termentzidis, Phys. Rev. B **89**, 054309 (2014).

[45] N. Mingo, Phys. Rev. B **74**, 125402 (2006).

[46] D. Singh, J. Murthy, and T. Fisher, J. Heat Transfer **133**, 122401 (2011).

[47] X. Ruan and M. Kaviany, J. Comput Theor Nanos **5**, 221 (2008).

[48] J. Kim and M. Kaviany, Phys. Rev. B **79**, 054103 (2009).

[49] J. Noffsinger, E. Kioupakis, C. G. Van de Walle, S. G. Louie, and M. L. Cohen, Phys. Rev. Lett. **108**, 167402 (2012).

[50] M. Trigo, J. Chen, V. H. Vishwanath, Y. M. Sheu, T. Graber, R. Henning, and D. A. Reis, Phys. Rev. B **82**, 235205 (2010).

[51] D. Song, F. Wang, G. Dukovic, M. Zheng, E. D. Semke, L. E. Brus, and T. F. Heinz, Phys. Rev. Lett. **100**, 225503 (2008).

[52] J. A. Kash, J. C. Tsang, and J. M. Hvam, Phys. Rev. Lett. **54**, 2151 (1985).

[53] K. T. Tsen, R. P. Joshi, D. K. Ferry, and H. Morkoc, Phys. Rev. B **39**, 1446 (1989).

[54] P. K. Schelling, S. R. Phillpot, and P. Keblinski, Appl. Phys. Lett. **80**, 2484 (2002).

[55] H. Kim and M. Kaviany, Phys. Rev. B **87**, 155133 (2013).

[56] M. Ikezawa and M. Ishigame, J. Phys. Soc. Jpn. **50**, 3734 (1981).

[57] N. A. Roberts and D. G. Walker, Int. J. Therm. Sci. **50**, 648 (2011).

[58] H. M. van Driel, in *Semiconductors Probed by Ultrafast Laser Spectroscopy*, Vol. 2, edited by R. R. Alfano (Academic, New York, 1984) p. 57.

[59] J. Fritsch, P. Pavone, and U. Schröder, Phys. Rev. B **52**, 11326 (1995).

[60] S.-F. Ren, W. Cheng, and P. Y. Yu, Phys. Rev. B **69**, 235327 (2004).

[61] M. Maldovan, Nature **503**, 209217 (2013).

[62] N. Li, J. Ren, L. Wang, G. Zhang, P. Hänggi, and B. Li, Rev. Mod. Phys. **84**, 1045 (2012).